ACS APPLIED MATERIALS & INTERFACES

Research Article

www.acsami.org

Inorganic Surface Engineering to Enhance Perovskite Solar Cell Efficiency

Naemeh Aeineh,[†,‡] Eva M. Barea,[†] Abbas Behjat,[‡] Nafiseh Sharifi,[§] and Iván Mora-Seró*[,†]

[†]Institute of Advanced Materials (INAM), Universitat Jaume I, Castelló 12006, Spain

[‡]Atomic and Molecular Division, Faculty of Physics, Yazd University, Yazd, Iran

[§]Physics Department, University of Kashan, Kashan 14588, Iran

Supporting Information

ABSTRACT: The photoconversion efficiency of perovskite solar cells (PSCs) is enhanced by the deposition of inorganic nanoparticles (NPs) at the interface between the compact TiO_2 electron-selective contact and the mesoporous TiO_2 film. The NPs used are core/shell Au@SiO_2, where a thin SiO_2 coating protects the Au core from the direct chemical interaction with $CH_3NH_3PbI_3$ halide perovskite used as light-harvesting material. The samples prepared with Au@SiO_2 NPs exhibit a higher external quantum efficiency in the complete wavelength range at which perovskite presents light absorption and not just at the wavelengths at which Au@SiO_2 NPs present their absorption peak. This fact rules out a direct plasmonic process as responsible for the enhancement of cell performance. A detailed characterization by photoluminescence, impedance spectroscopy, and open-circuit voltage decay unveils a modification of the interfacial properties with an augmentation of the interfacial electrostatic potential that increases both photovoltage and photocurrent. This article highlights the dramatic role of interfaces in the performance of PSCs. The use of reduced quantities of highly stable inorganic compounds to modify the PSC interface instead of the extensively used organic compounds opens the door to a new surface engineering based on inorganic compounds.

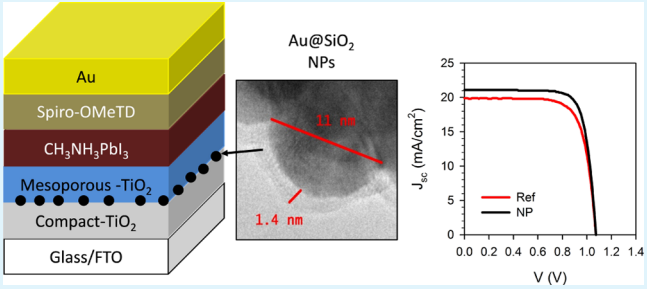

KEYWORDS: *Perovskite, solar cell, surface engineering, Au@SiO_2, inorganic*

1. INTRODUCTION

The actual requirement of clean energy imposes to the society an important endeavor, involving a huge effort to develop suitable renewable energy sources. The photovoltaic energy is a promising candidate, and particularly perovskite solar cells have attracted much interest recently because of their high efficiency, low cost, and simple manufacturing.[1,2] Since the seminal report from Miyasaka's group, where $CH_3NH_3PbI_3$ perovskite was used as the light harvester in a liquid-state perovskite-sensitized solar cell, reporting a power conversion efficiency (PCE) of 3.8%,[3] the PCE of perovskite solar cells (PSCs) has improved rapidly up to 22% in 2016.[4]

Although the improvement in efficiency in recent years has been spectacular, there are many aspects of the device that can be further improved, in terms of not only efficiency but also stability. One of the key points of the perovskite solar cell performance is the role of the interfaces at charge-selecting contacts. The use of appropriate selecting contacts between the perovskite layer and extracting contacts, transparent conductive oxide and Au in most of the cases, allows to decrease significantly the interface recombination, thereby increasing the cell efficiency.[5,6] In addition, interfaces also play an important role on the high stability of the device[7,8] and on other characteristic properties of perovskite solar cells as hysteresis.[9−13] Interestingly, the interface properties can be significantly tuned not just by the addition of an extra layer between the perovskite and the selecting contact but simply with the use of a self-assembled monolayer. This possibility of interface engineering has been extensively studied for organic molecules, for example, using fullerene derivatives deposited at the TiO_2−perovskite interface.[10,12,13] However, the use of inorganic systems for surface engineering in PSCs has been less studied and reduced in most of the cases to the deposition of a thin coating layer.[14,15] For example, it has been reported that the use of mesoporous layers coated with an ultrathin MgO layer reduces the recombination in PSCs,[15] and the deposition of a thin alumina layer at the electron-selecting contact increases the external quantum efficiency of perovskite LEDs.[16]

In this study, we use gold nanoparticles (NPs) coated with a thin SiO_2 shell. The use of small Au-core NPs (diameter, ∼11 nm) has allowed us to prepare small core/shell Au@SiO_2 NPs (diameter, ∼14 nm; Figure 1a). Metallic nanoparticles have been extensively studied in solution-processed solar cells because of their plasmonic properties.[17,18] In the case of

Received: January 25, 2017
Accepted: March 29, 2017
Published: March 29, 2017

DOI: 10.1021/acsami.7b01306
ACS Appl. Mater. Interfaces 2017, 9, 13181−13187

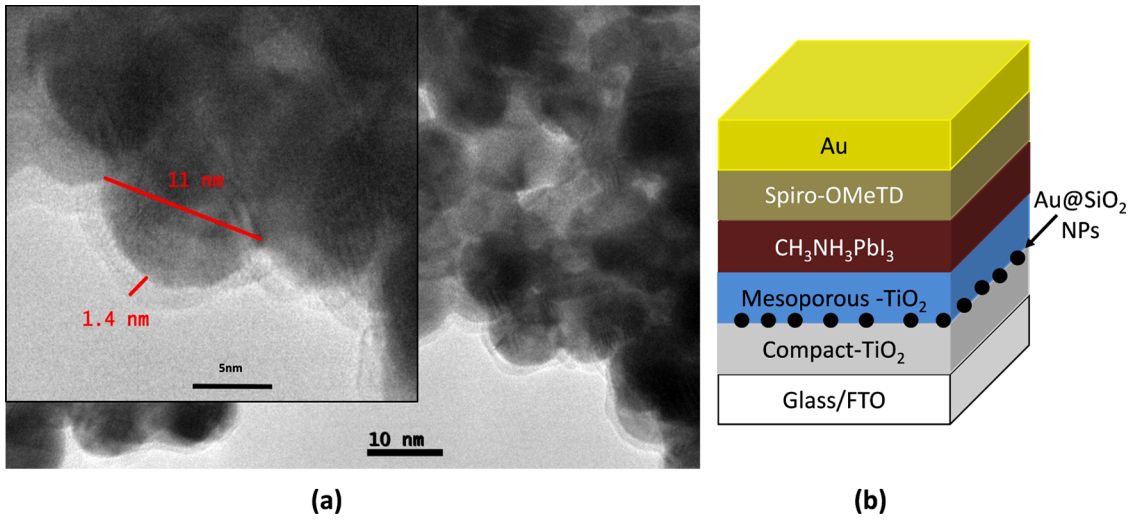

Figure 1. (a) Transmission electron microscopy (TEM) image of Au NPs (inset: zoom-in image allowing an easy determination of the sizes of the Au core and the SiO_2-coated layer). (b) Schematic illustration of the structure of perovskite solar cells with spin coating of the Au NP from a concentrated solution on the top of compact TiO_2 film, just before mesoporous TiO_2 (mp-TiO_2).

PSCs, to ensure chemical stability, the direct contact between the halogen forming the perovskite and the Au has to be avoided. The physical separation of perovskite and Au is obtained by the use of TiO_2 or SiO_2[19,20] shells coated with gold core or embedding Au NPs on a compact titania-selective layer.[21] It has been reported that PSCs fabricated using core/shell plasmonic NPs[19,20,22] or selective contact layers with embedded Au NPs[21] produce devices with a higher PCE than that of the corresponding reference cells prepared in the same way but without metallic NPs. Theory predicts that a wavelength selectivity increases the solar cell performance owing to the plasmonic enhancement of light absorption at the wavelengths at which metallic NPs exhibit the absorption peak.[23,24] However, the real role of plasmonics on the enhancement of PCE observed for PSCs is under debate, as no-wavelength selectivity is observed, but devices present a general improvement of performance in the broad wavelength absorption range of perovskite and not just in the region of plasmonic absorption.[19−22] Snaith and co-workers proposed a plasmonic-induced photon recycling to explain this apparent contradiction.[22] Moreover, Au NPs should have a radius higher than 10 nm to produce an observable effect on light absorption.[23,24] As it has been commented, the Au@SiO_2 NPs studied here (diameter, ∼14 nm) are significantly smaller that those employed in previous studies (80 nm).[19] Consequently, no plasmonic effect is expected for the size of the employed Au-core NPs used in this study. Nevertheless, the modification of the interface between the compact TiO_2-selective layer and the perovskite film by the deposition of Au@SiO_2 produces an increase in the performance of PSCs. We show that this enhancement is not due to the plasmonic effect but due to the modification of the interface charge-transfer properties.

2. EXPERIMENTAL SECTION

2.1. NP Synthesis. A gold solution (500 mL, 5×10^{-4} M$HAuCl_4$) is prepared according to the Turkevich procedures.[25] To 250 mL of $HAuCl_4$ solution (1 mM), 25 mL of 1% sodium citrate solution was added, with boiling and vigorous stirring. After continuous boiling for 10 min, the mixture was allowed to cool. This method produces a stable, deep-red dispersion of gold particles with an average diameter of about 11 nm (Figure 1a). Au@SiO_2 core/shell NPs were prepared according to the synthetic protocol of Liz-Marzán and co-workers.[26] Briefly, freshly prepared 1 mM aqueous solution of (3-aminopropyl)-trimethoxysilane (APS) (2.5 mL) was added to 500 mL of the gold solution under vigorous magnetic stirring. The mixture was stirred for 15 min to ensure complete complexation of the amine groups with the gold surface. Then, a solution of active silica was prepared by lowering the pH of a 0.54 wt % sodium silicate solution. The active silica (20 mL) was added to 500 mL of the surface-modified gold solution again under vigorous magnetic stirring. After stirring for 24 h, the NPs were collected by centrifugation at 15 000 rpm for 1 h, washed three times with deionized water, and finally redispersed in ethanol. The thickness of the silica shell is about 1.4 nm (Figure 1a).

2.2. Substrates. SnO_2:F (FTO) substrates were cleaned with soap; sonicated in distilled water, ethanol, and a mixture of acetone/isopropanol (30:70 v/v ratio) for 15 min; and treated with a UV−O_3 lamp for 15 min. The TiO_2 compact layer was deposited by spray pyrolysis at 450 °C, consuming 28 mL of a solution of titanium di-isopropoxide bis(acetylacetonate, 75 vol % 2-propanol) in absolute ethanol (1:39, v/v ratio); the films were annealed at 450 °C for 30 min. Core/shell nanoparticles of Au@SiO_2 in ethanol were embedded by spin coating on the compact layer at 2000 rpm for 30 s and drying at 100 °C for 10 min. Different concentrations of NPs were evaluated, and the best results were obtained for 200 μL of Au@SiO_2 solution in 1 mL of Et-OH (Table S1). A lower NP concentration is not enough to enhance the efficiency, and a higher NP concentration produces a larger surface coating of the TiO_2-selective contact with isolating NPs that hinder the charge injection at the interface. The mp-TiO_2 layer (commercial Dyesol 30NR-D TiO_2 paste with 30 nm TiO_2 NPs) in ethanol (1:5 in weight) was deposited on the top of the TiO_2 compact layer by spin coating at 2000 rpm for 10 s. After drying at 100 °C for 10 min, the layer was annealed in air up to 500 °C for 30 min. Then, a 35 mM solution of lithium bis-(strifluoromethanesulfonamide) (LiTFSI) in acetonitrile was deposited by spin coating onto the substrates at 3000 rpm for 10 s. Then, the films were annealed at 450 °C for 30 min.[27] Reference samples with no NPs were prepared in the same way but without the Au@SiO_2 deposition step.

2.3. Au@SiO_2 NPs Incorporated into mp-TiO_2. Au@SiO_2 NPs have also been incorporated into mp-TiO_2 paste to evaluate the effect of the placement of NPs on the final cell performance. Different concentrations of Au@SiO_2 NP solution in ethanol (20, 40, 60, 80, and 100 μL) were mixed with 1 mL of dilute commercial TiO_2 paste (30NR-D, Dyesol) in ethanol (weight ratio, 1:5) and stirred overnight. The Au@SiO_2/TiO_2 (mp-TiO_2) layer was deposited on the bl-TiO_2

DOI: 10.1021/acsami.7b01306
ACS Appl. Mater. Interfaces 2017, 9, 13181−13187

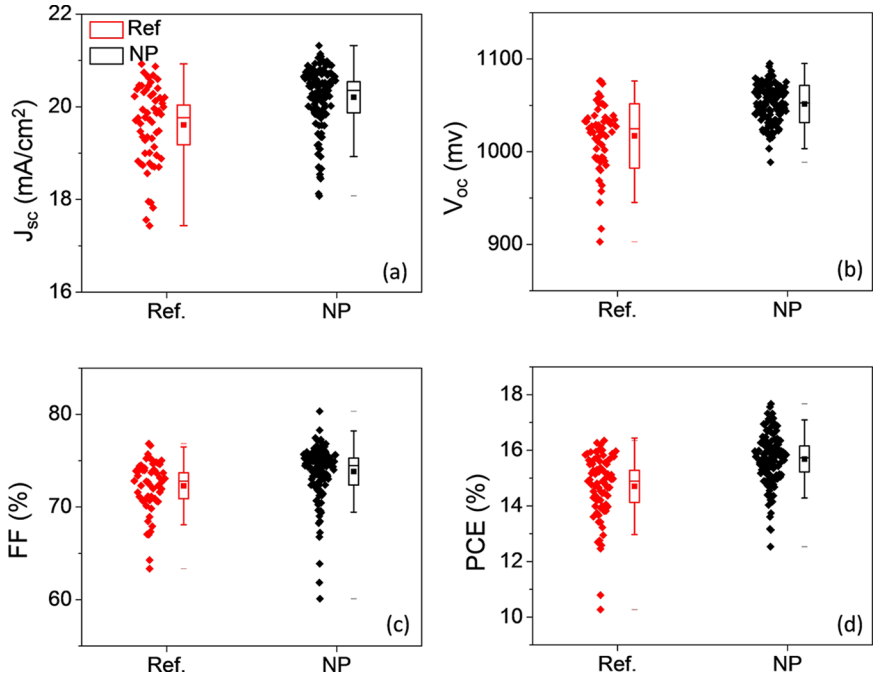

Figure 2. Statistics of the photovoltaic performance of 50 individual devices (red: reference cells; black: devices with NPs). (a) Short-circuit current density, (b) open-circuit voltage, (c) fill factor, and (d) PCE plotted for cells with and without interfacial NPs. The error bars represent plus or minus one standard deviation from the mean.

by spin coating at 2000 rpm for 10 s. After drying at 100 °C for 10 min, the layer was annealed in air up to 500 °C for 30 min.

2.4. Perovskite Solution. PbI_2 (622 mg, 1.35 mmol) was added to a solution containing 1 mL of DMF and 95 μL of dimethyl sulfoxide (DMSO). This solution was heated at 65 °C to dissolve PbI_2 and then cooled to room temperature. Subsequently, the PbI_2 solution was poured into a vial containing 215 mg (1.35 mmol) of MAI to obtain the final solution for the perovskite deposition at 4000 rpm and 50 s; at 5 s, diethyl ether was dripped on the rotating substrate before the surface changes, to prevent the faster evaporation of DMF.[28] After deposition, the film was heated at 65 °C for 3 min to obtain a dense $CH_3NH_3PbI_3$ film.

2.5. Spiro-OMeTAD and Gold. The Spiro-OMeTAD solution was prepared by dissolving 72.3 mg of spiro-OMeTAD(2,2′,7,7′-tetrakis(*N*,*N*-di-*p*-methoxyphenylamine)-9,9-spirobifluorene) in 1 mL of chlorobenzene and then mixing it with 28.8 μL of 4-*tert*-butylpyridine and 17.5 μL of a stock Li+ solution (which contained 520 mg/mL bistrifluoromethylsulfonylamine lithium salt in acetonitrile). The Spiro-OMeTAD layer was spin-coated on perovskite films at 4000 rpm for 30 s. Finally, 60 nm of gold was thermally evaporated in an ultrahigh vacuum chamber on the top of Spiro-OMeTAD layer to make complete devices.

2.6. Characterization. The Au NPs were characterized by TEM JEOL 2100. The absorbance data were obtained by using a Varian Cary 300 Bio spectrophotometer. Photoluminescence was obtained using a fluorimeter Horiba FL-100. All of the devices were characterized by current−potential (*J*−*V*) curves measured under 1 sun (AM 1.5G; 100 mW cm^{-2}) using a Sun 2000 system solar simulator from Abet Technologies. The impedance and open-circuit voltage decay (OCVD) measurements were carried out in a PGSTAT-30 potentiostat from Autolab. The OCVD measurements were performed after light-soaking preconditioning for 5 min.

3. RESULT AND DISCUSSION

We have prepared PSCs using the most standard architecture with compact TiO_2 and spiro-OMeTAD as electron- and hole-selective contacts, respectively, and with a TiO_2 mesoporous scaffold.[29] $CH_3NH_3PbI_3$ hybrid organic−inorganic halide perovskite has been used as the light-harvesting layer. This standard configuration has been modified by adding Au@SiO_2 core/shell nanoparticles between the TiO_2 compact layer and the mesoporous layer. The configuration of perovskite solar cells with NPs is shown in Figure 1b.

The performance of the perovskite solar cells prepared with and without Au@SiO_2 NPs (reference), denoted as NP and Ref, respectively, has been systematically characterized to investigate the effectiveness of NPs in the increase of solar cell performance. More than 50 solar cells have been prepared under each condition. A statistical analysis of the photovoltaic parameters of the fabricated samples is shown in Figure 2. It can be compared with the statistical features of short-circuit current density (J_{sc}), open-circuit voltage (V_{oc}), fill factor (FF), and PCE of all of the cells with and without NPs. It can be clearly appreciated that the average values of V_{oc}, J_{sc}, FF are increased when NPs are introduced in the devices, thereby leading to an increase in the average PCE. Table 1 summarizes the average values of the photovoltaic parameters, showing also the performance of the champion solar cells obtained with and without Au@SiO_2. The cells with NPs exhibit higher

Table 1. Average Values of V_{oc}, J_{sc}, FF, and PCE, along with Their Standard Deviations, for Perovskite Solar Cells with and without Au@SiO_2 NPs under the Irradiation of 1 sun Intensity (100 mW cm^{-2}; AM 1.5G)[a]

samples	J_{SC} (mA/cm^2)	V_{oc} (mV)	FF (%)	PCE (%)
Ref	19.6 ± 0.9	1017 ± 34	72 ± 3	14.4 ± 1.0
Ref (champion)	19.86	1076	75.71	16.18
with NP	20.5 ± 0.7	1051 ± 20	74 ± 3	16.0 ± 0.9
with NP (champion)	20.73	1081	78.29	17.55

[a]The concentration of the Au@SiO_2 NP solution used for the NP deposition has been previously optimized using a smaller number of cell devices (Table S1).

DOI: 10.1021/acsami.7b01306
ACS Appl. Mater. Interfaces 2017, 9, 13181−13187

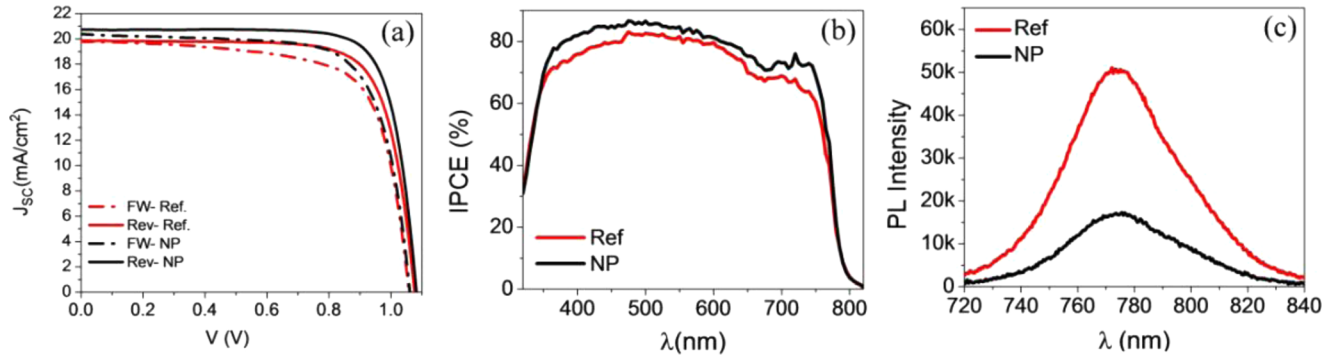

Figure 3. (a) J–V curve measured under 1 sun illumination for the champion devices with forward (FW) and reserve (Rev) voltage scans. (b) Incident photon to current efficiency (IPCE) spectra and (b) photoluminescence (PL) intensity of devices with and without interfacial NPs.

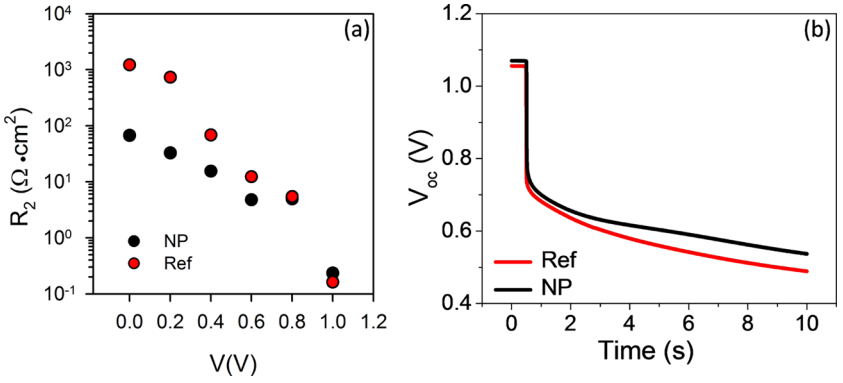

Figure 4. (a) Resistance at intermediate frequency (R_2) as a function of voltage obtained from the fitting of the IS spectra using the equivalent circuit plotted in Figure S4.[31] (b) OCVD as a function of loading for perovskite solar cell with and without interfacial NPs measured after light-soaking preconditioning.

photovoltaic parameters, that is, higher performance, lower standard deviation, and higher reproducibility. The record PCE obtained for solar cells with NPs was 17.55% (J_{sc} = 20.73 mA/cm^2, V_{oc} =1.081 V, and FF = 0.782) higher than that obtained for devices without NPs, which present 16.18% record PCE (Table 1). J–V curves of champion cells are plotted in Figure 3a. As far as we know, this efficiency is the highest one reported for PSCs using nanoparticles based on metallic structures. The use of interfacial Au@SiO_2 NPs does not have a significant effect on the hysteresis of the samples in comparison with reference cells (Figure 3a). Only a slight decrease of the hysteresis index from 0.038 to 0.035 is observed for cells with and without interfacial NPs, respectively. The hysteresis index presents a value of zero when no hysteresis is present and one when the difference of the photocurrents between the forward and reverse scans at a voltage half the open-circuit voltage is as high as the photocurrent of the reverse scan.[30]

To compare with previous works in which Au@SiO_2 NPs were embedded in the mesoporous scaffold,[19−22] solar cells without NPs at the interface but with NPs mixed in the scaffold in different concentrations have been prepared. The solar cell parameters are displayed in Table S2. For low concentration of NPs, no significant difference with the reference cells, considering the standard deviation, can be appreciated. However, for Au@SiO_2 NPs with concentrations higher than 60 μL incorporated into 1 mL of the mp-TiO_2 paste, a clear decrease in performance is appreciated (Table S2). This study clearly highlights that the observed enhancement of PCE in Table 1 is because of not only the use of Au@SiO_2 NPs but also the interfacial placement on these NPs.

To understand the increase in the efficiency of the devices with interfacial NPs, further optoelectronic characterization has been performed. A comparison of the IPCE between samples with and without nanoparticles is depicted in Figure 3b. Although Au@SiO_2 NPs present an absorption peak at 500–650 nm wavelength (Figure S1), the recorded IPCE does not exhibit this wavelength selectivity. When NPs are added at the interface between the TiO_2 compact layer and the mesoporous layers, an increase over the whole reference perovskite wavelength light absorption range (350–770 nm) is observed (Figure 3b). In addition, no significant change is observed in the light absorption at the 500–650 nm wavelength region of compact/mp-TiO_2 layers with and without interfacial Au@SiO_2 NPs (Figure S2). These observations rule out a direct plasmonic effect by an increase of light absorption in the solar cell enhancement observed when NPs are used at the interface. Interestingly, the addition of NPs at the interface produces a strong quenching of the perovskite PL, see Figure 3c. It has been previously reported a slight quenching of PL in PSCs with the addition of Ag/TiO_2 NPs.[22] However, it that case, less than a twofold decrease was reported, whereas here a fivefold PL reduction is observed after the introduction of NPs. PL quenching after the modification of the selective contacts has been explained by an increase of the electron injection at the perovskite–electron-selective contact. The faster injection of photogenerated electrons into the TiO_2-selecting contact presenting a self-assembled monolayer of fullerene derivatives reduces the radiative recombination in the perovskite layer with the consequent reduction in PL.[10,13] In the same way, we show that the surface engineering of the TiO_2–perovskite interface

DOI: 10.1021/acsami.7b01306
ACS Appl. Mater. Interfaces 2017, 9, 13181–13187

by inorganic Au@SiO_2 NPs presents an analogous behavior pointing to an interfacial effect as the origin of the efficiency enhancement obtained when NPs are added.

To characterize the interfacial properties of the fabricated samples, Impedance Spectroscopy (IS) and OCVD have been employed. Both the techniques have demonstrated a strong sensitivity to interfacial processes on PSCs.[5,6,14,31−34] IS is a very useful characterization technique, as it allows to decouple the different processes occurring in a complete device if they present different characteristic times.[35] In the case of PSCs, impedance spectra are mostly governed by interfacial rather than bulk processes.[6] The PSC impedance pattern presents several features, basically two to three arcs at different frequency ranges.[5,6,31,33] It has been reported that the observed arc at intermediate frequencies is directly influenced by the electron-selective contact interface. The characteristic resistance of this arc at intermediate frequencies, hereafter labeled R_2, strongly depends on the kind of oxide used as selective contact;[31] furthermore, there is a reverse correlation between R_2 and the obtained photocurrent, increasing J_{sc} when R_2 decreases.[31,32] In good agreement with these previous observations, we observe lower R_2 values for samples with Au@SiO_2 NPs, which also present a higher photocurrent (Figure 4a). This fact points to an increase of the charge extraction at the interface modified by the NPs in good agreement with the PL quenching observed (Figure 3c). The Nyquist plot of the analyzed samples is depicted in Figure S3. The IS spectra in Figure S3 have been fitted using the equivalent circuit plotted in Figure S4.[31] R_2 is the only parameter that presents a significant variation comparing reference cells and cells prepared from Au@SiO_2 NPs (Figure S5).

We have also carried out OCVD measurements on both kinds of samples to reinforce this hypothesis. Figure 4b shows OCVD characteristics of devices with and without interfacial NPs. As it has been previously reported, two regions with different behaviors can be distinguished at short and long times. At short times, fast decay is produced by the interfacial recombination, whereas a slower decay is observed especially after light-soaking preconditioning of the sample before the OCVD measurement.[14] Light soaking produces ion migration with an accumulation of cations and majority holes at the electron-selective contact interface, producing a net interfacial electric field and consequently building up an electrostatic interfacial potential, V_{elec} (Figure S6). The use of mp-TiO_2 layer is supposed not to affect severely the field distribution.[14,36] Consequently, the open-circuit voltage observed with illumination preconditioning presents two contributions, $V_{oc} = V_{bi} + V_{elec}$, one from the built-in potential (V_{bi}) and another from the electrostatic potential (V_{elec}). In an OCVD measurement, when the illumination producing V_{oc} is switched off, the V_{bi} is removed rapidly, at times shorter than 1 s (Figure 4b), owing to the electron−hole recombination, whereas removing V_{elec} requires much longer times, as this process is governed by the slower ion migration, which eliminates the interfacial ion accumulation produced by the illumination.[14] As a result, OCVD is ruled by the interfacial processes and it is an excellent tool to characterize the device interface. In Figure 4b, at longer times, it can be observed that samples with NPs present a higher V_{oc}, indicating that the presence of NPs affects the interfacial electrostatic potential, enhancing the V_{oc} of samples with Au@SiO_2 NPs (Figure S6). On the other hand, the presence of majority hole accumulation produces a strong band bending at perovskite−electron-selective contact interface, as it has been described by Zarazua et al.[6,37] and very recently confirmed by Bergmann et al.[38] and Chen et al. using different methods.[39] This band bending reveals that electronic charge injection at electron-selective contact occurs via tunneling.[39] As a result, the electric field formed at the interface due to the cation and hole accumulation that produce the band bending[14] also influences the charge-transfer properties via tunneling and consequently the photocurrent (Figure S6), explaining the increase of J_{sc} observed when Au@SiO_2 NPs are added at the interface.

4. CONCLUSIONS

We have embedded small (∼14 nm) core/shell Au/SiO_2 NPs by spin coating at the interface between compact TiO_2 and mp-TiO_2 used as substrates for the preparation of perovskites solar cells. Statistically significant data were obtained, showing an improvement in PCE primarily due to the enhancement in photocurrent. Under the best conditions, the cells with NPs show a PCE of 17.55%, which is higher than the PCE of 16.18% obtained for reference cells with no NPs. The observed enhancement in photocurrent does not exhibit the wavelength selectivity expected from a light absorption increase owing to a plasmonic effect, in good agreement with theoretical predictions for small NPs as the ones used in this work. This fact rules out the possibility of solar cell enhancement by an increase of light absorption. Further characterization by photoluminescence, IS, and OCVD points to an interfacial effect as the origin of the increase of solar cell performance. The presence of Au@SiO_2 NPs increases the electrostatic potential produced at the electron-selective contact under illumination with beneficial implications for photovoltage and photocurrent. The band bending produced by cation and hole accumulation at the electron-selective contact under illumination produces an increase of V_{oc} and J_{sc} due to the enhanced electrostatic potential and the increased charge injection at the interface by tunneling effect. From the fundamental point of view, this study emphasizes the dramatic role of interfaces in PSCs. From the applied point of view, interestingly, in the present study, inorganic NPs with long-term stability have been employed, paving the way for an advanced surface engineering that is able to affect the interfacial properties enhancing cell performance and preserving cell stability.

■ ASSOCIATED CONTENT

Supporting Information

The Supporting Information is available free of charge on the ACS Publications website at DOI: 10.1021/acsami.7b01306.

Light absorption of a suspension of Au@SiO_2 NPs; optical absorption with and without interfacial NPs; Nyquist plot with and without interfacial NPs; equivalent circuit employed for impedance spectra fitting; values obtained from the fitting of the impedance spectra; energy diagram schemes; solar cell parameters of devices with different concentrations of interfacial NPs and with different concentrations of NPs mixed in the TiO_2 scaffold (PDF)

■ AUTHOR INFORMATION

Corresponding Author

*E-mail: sero@uji.es.

DOI: 10.1021/acsami.7b01306
ACS Appl. Mater. Interfaces 2017, 9, 13181−13187

ORCID

Iván Mora-Seró: 0000-0003-2508-0994

Notes

The authors declare no competing financial interest.

■ ACKNOWLEDGMENTS

This study was supported by MINECO of Spain (project MAT2016-76892-C3-1-R) , Generalitat Valenciana (project PROMETEOII/2014/020) and SOLENPE (project UJI-B2016-35). The authors acknowledge SCIC from University Jaume I for help in TEM characterization. N.A. thanks Iranian Ministry of Science and Technology (Tehran, Iran) and Yazd University for supporting her visit to the Institute of Advanced Materials (INAM) at Universitat Jaume I (Spain).

■ REFERENCES

(1) Park, N.-G.; Grätzel, M.; Miyasaka, T.; Zhu, K.; Emery, K. Towards Stable and Commercially Available Perovskite Solar Cells. *Nat. Energy* **2016**, *1*, No. 16152.

(2) Brenner, T. M.; Egger, D. A.; Kronik, L.; Hodes, G.; Cahen, D. Hybrid Organic-Inorganic Perovskites: Low-Cost Semiconductors with Intriguing Charge-Transport Properties. *Nat. Rev. Mater.* **2016**, *1*, No. 15007.

(3) Kojima, A.; Teshima, K.; Shirai, Y.; Miyasaka, T. Organometal Halide Perovskites as Visible-Light Sensitizers for Photovoltaic Cells. *J. Am. Chem. Soc.* **2009**, *131*, 6050−6051.

(4) Green, M. A.; Emery, K.; Hishikawa, Y.; Warta, W.; Dunlop, E. D. Solar Cell Efficiency Tables (Version 48). *Prog. Photovoltaics* **2016**, *24*, 905−913.

(5) Juarez-Perez, E. J.; Wußler, M.; Fabregat-Santiago, F.; Lakus-Wollny, K.; Mankel, E.; Mayer, T.; Jaegermann, W.; Mora-Sero, I. Role of the Selective Contacts in the Performance of Lead Halide Perovskite Solar Cells. *J. Phys. Chem. Lett.* **2014**, *5*, 680−685.

(6) Zarazua, I.; Han, G.; Boix, P. P.; Mhaisalkar, S.; Fabregat-Santiago, F.; Mora-Seró, I.; Bisquert, J.; Garcia-Belmonte, G. Surface Recombination and Collection Efficiency in Perovskite Solar Cells from Impedance Analysis. *J. Phys. Chem. Lett.* **2016**, *7*, 5105−5113.

(7) Sanchez, R. S.; Mas-Marza, E. Light-Induced Effects on Spiro-OMeTAD Films and Hybrid Lead Halide Perovskite Solar Cells. *Sol. Energy Mater. Sol. Cells* **2016**, *158*, 189−194.

(8) Govindhasamy, M.; Soichiro, T.; Gai, M.; Shusaku, K.; Hitoshi, N.; Tomokazu, U.; Hiroshi, I.; Seigo, I. Light Stability Tests of Methylammonium and Formamidinium Pb-Halide Perovskites for Solar Cell Applications. *Jpn. J. Appl. Phys.* **2015**, *54*, No. 08KF08.

(9) Snaith, H. J.; Abate, A.; Ball, J. M.; Eperon, G. E.; Leijtens, T.; Noel, N. K.; Stranks, S. D.; Wang, J. T.-W.; Wojciechowski, K.; Zhang, W. Anomalous Hysteresis in Perovskite Solar Cells. *J. Chem. Phys. Lett.* **2014**, *5*, 1511−1515.

(10) Wojciechowski, K.; Stranks, S. D.; Abate, A.; Sadoughi, G.; Sadhanala, A.; Kopidakis, N.; Rumbles, G.; Li, C.-Z.; Friend, R. H.; Jen, A. K. Y.; Snaith, H. J. Heterojunction Modification for Highly Efficient Organic−Inorganic Perovskite Solar Cells. *ACS Nano* **2014**, *8*, 12701−12709.

(11) Levine, I.; Nayak, P. K.; Wang, J. T.-W.; Sakai, N.; van Reenen, S.; Brenner, T. M.; Mukhopadhyay, S.; Snaith, H. J.; Hodes, G.; Cahen, D. Interface-Dependent Ion Migration/Accumulation Controls Hysteresis in MAPbI3 Solar Cells. *J. Chem. Phys. C* **2016**, *120*, 16399.

(12) Tao, C.; Neutzner, S.; Colella, L.; Marras, S.; Srimath Kandada, A. R.; Gandini, M.; Bastiani, M. D.; Pace, G.; Manna, L.; Caironi, M.; Bertarelli, C.; Petrozza, A. 17.6% Stabilized Efficiency in Low-Temperature Processed Planar Perovskite Solar Cells. *Energy Environ. Sci.* **2015**, *8*, 2365−2370.

(13) Valles-Pelarda, M.; Hames, B. C.; García-Benito, I.; Almora, O.; Molina-Ontoria, A.; Sánchez, R. S.; Garcia-Belmonte, G.; Martín, N.; Mora-Sero, I. Analysis of the Hysteresis Behavior of Perovskite Solar Cells with Interfacial Fullerene Self-Assembled Monolayers. *J. Phys. Chem. Lett.* **2016**, *7*, 4622−4628.

(14) Gottesman, R.; Lopez-Varo, P.; Gouda, L.; Jimenez-Tejada, J. A.; Hu, J.; Tirosh, S.; Zaban, A.; Bisquert, J. Dynamic Phenomena at Perovskite/Electron-Selective Contact Interface as Interpreted from Photovoltage Decays. *Chem* **2016**, *1*, 776−789.

(15) Han, G. S.; Chung, H. S.; Kim, B. J.; Kim, D. H.; Lee, J. W.; Swain, B. S.; Mahmood, K.; Yoo, J. S.; Park, N.-G.; Lee, J. H.; Jung, H. S. Retarding Charge Recombination in Perovskite Solar Cells Using Ultrathin MgO-Coated TiO_2 Nanoparticulate Films. *J. Mater. Chem. A* **2015**, *3*, 9160−9164.

(16) Tan, Z.-K.; Moghaddam, R. S.; Lai, M. L.; Docampo, P.; Higler, R.; Deschler, F.; Price, M.; Sadhanala, A.; Pazos, L. M.; Credgington, D.; Hanusch, F.; Bein, T.; Snaith, H. J.; Friend, R. H. Bright Light-Emitting Diodes Based on Organometal Halide Perovskite. *Nat. Nanotechnol.* **2014**, *9*, 687−692.

(17) Arinze, E. S.; Qiu, B.; Nyirjesy, G.; Thon, S. M. Plasmonic Nanoparticle Enhancement of Solution-Processed Solar Cells: Practical Limits and Opportunities. *ACS Photonics* **2016**, *3*, 158−173.

(18) Nourolahi, H.; Behjat, A.; Hosseini Zarch, S. M. M.; Bolorizadeh, M. A. Silver Nanoparticle Plasmonic Effects on Hole-Transport Material-Free Mesoporous Heterojunction Perovskite Solar Cells. *Sol. Energy* **2016**, *139*, 475−483.

(19) Zhang, W.; Saliba, M.; Stranks, S. D.; Sun, Y.; Shi, X.; Wiesner, U.; Snaith, H. J. Enhancement of Perovskite-Based Solar Cells Employing Core−Shell Metal Nanoparticles. *Nano Lett.* **2013**, *13*, 4505−4510.

(20) Pathak, N. K.; Chander, N.; Komarala, V. K.; Sharma, R. P. Plasmonic Perovskite Solar Cells Utilizing Au@SiO2 Core-Shell Nanoparticles. *Plasmonics* **2016**, No. 237.

(21) Yuan, Z.; Wu, Z.; Bai, S.; Xia, Z.; Xu, W.; Song, T.; Wu, H.; Xu, L.; Si, J.; Jin, Y.; Sun, B. Hot-Electron Injection in a Sandwiched TiO_x−Au−TiO_x Structure for High-Performance Planar Perovskite Solar Cells. *Adv. Energy Mater.* **2015**, *5*, No. 1500038.

(22) Saliba, M.; Zhang, W.; Burlakov, V. M.; Stranks, S. D.; Sun, Y.; Ball, J. M.; Johnston, M. B.; Goriely, A.; Wiesner, U.; Snaith, H. J. Plasmonic-Induced Photon Recycling in Metal Halide Perovskite Solar Cells. *Adv. Funct. Mater.* **2015**, *25*, 5038−5046.

(23) Carretero-Palacios, S.; Calvo, M. E.; Míguez, H. Absorption Enhancement in Organic−Inorganic Halide Perovskite Films with Embedded Plasmonic Gold Nanoparticles. *J. Phys. Chem. C* **2015**, *119*, 18635−18640.

(24) Carretero-Palacios, S.; Jiménez-Solano, A.; Míguez, H. Plasmonic Nanoparticles as Light-Harvesting Enhancers in Perovskite Solar Cells: A User's Guide. *ACS Energy Lett.* **2016**, *1*, 323−331.

(25) Enustun, B. V.; Turkevich, J. Coagulation of Colloidal Gold. *J. Am. Chem. Soc.* **1963**, *85*, 3317−3328.

(26) Liz-Marzán, L. M.; Giersig, M.; Mulvaney, P. Synthesis of Nanosized Gold−Silica Core−Shell Particles. *Langmuir* **1996**, *12*, 4329−4335.

(27) Giordano, F.; Abate, A.; Correa Baena, J. P.; Saliba, M.; Matsui, T.; Im, S. H.; Zakeeruddin, S. M.; Nazeeruddin, M. K.; Hagfeldt, A.; Graetzel, M. Enhanced Electronic Properties in Mesoporous TiO_2 Via Lithium Doping for High-Efficiency Perovskite Solar Cells. *Nat. Commun.* **2016**, *7*, No. 10379.

(28) Ahn, N.; Son, D.-Y.; Jang, I.-H.; Kang, S. M.; Choi, M.; Park, N.-G. Highly Reproducible Perovskite Solar Cells with Average Efficiency of 18.3% and Best Efficiency of 19.7% Fabricated via Lewis Base Adduct of Lead(II) Iodide. *J. Am. Chem. Soc.* **2015**, *137*, 8696−8699.

(29) Kim, H.-S.; Lee, C.-R.; Im, J.-H.; Lee, K.-B.; Moehl, T.; Marchioro, A.; Moon, S.-J.; Humphry-Baker, R.; Yum, J.-H.; Moser, J. E.; Gratzel, M.; Park, N.-G. Lead Iodide Perovskite Sensitized All-Solid-State Submicron Thin Film Mesoscopic Solar Cell with Efficiency Exceeding 9%. *Sci. Rep.* **2012**, *2*, No. 591.

(30) Sanchez, R. S.; Gonzalez-Pedro, V.; Lee, J.-W.; Park, N.-G.; Kang, Y. S.; Mora-Sero, I.; Bisquert, J. Slow Dynamic Processes in Lead Halide Perovskite Solar Cells. Characteristic Times and Hysteresis. *J. Phys. Chem. Lett.* **2014**, *5*, 2357−2363.

(31) Guerrero, A.; Garcia-Belmonte, G.; Mora-Sero, I.; Bisquert, J.; Kang, Y. S.; Jacobsson, T. J.; Correa-Baena, J.-P.; Hagfeldt, A. Properties of Contact and Bulk Impedances in Hybrid Lead Halide

DOI: 10.1021/acsami.7b01306
ACS Appl. Mater. Interfaces 2017, 9, 13181−13187

Perovskite Solar Cells Including Inductive Loop Elements. *J. Phys. Chem. C* **2016**, *120*, 8023−8032.
(32) Anaya, M.; Zhang, W.; Hames, B. C.; Li, Y.; Fabregat-Santiago, F.; Calvo, M. E.; Snaith, H. J.; Miguez, H.; Mora-Sero, I. Electron Injection and Scaffold Effects in Perovskite Solar Cells. *J. Mater. Chem. C* **2017**, *5*, 634−644.
(33) Dualeh, A.; Moehl, T.; Tétreault, N.; Teuscher, J.; Gao, P.; Nazeeruddin, M. K.; Grätzel, M. Impedance Spectroscopic Analysis of Lead Iodide Perovskite-Sensitized Solid-State Solar Cells. *ACS Nano* **2014**, *8*, 362−373.
(34) Bertoluzzi, L.; Sanchez, R. S.; Liu, L.; Lee, J.-W.; Mas-Marza, E.; Han, H.; Park, N.-G.; Mora-Sero, I.; Bisquert, J. Cooperative Kinetics of Depolarization in $CH_3NH_3PbI_3$ Perovskite Solar Cells. *Energy Environ. Sci.* **2015**, *8*, 910−915.
(35) Fabregat-Santiago, F.; Garcia-Belmonte, G.; Mora-Seró, I.; Bisquert, J. Characterization of Nanostructured Hybrid and Organic Solar Cells by Impedance Spectroscopy. *Phys. Chem. Chem. Phys.* **2011**, *13*, 9083−9118.
(36) Jiang, C.-S.; Yang, M.; Zhou, Y.; To, B.; Nanayakkara, S. U.; Luther, J. M.; Zhou, W.; Berry, J. J.; van de Lagemaat, J.; Padture, N. P.; Zhu, K.; Al-Jassim, M. M. Carrier Separation and Transport in Perovskite Solar Cells Studied by Nanometre-Scale Profiling of Electrical Potential. *Nat. Commun.* **2015**, *6*, No. 8397.
(37) Zarazua, I.; Bisquert, J.; Garcia-Belmonte, G. Light-Induced Space-Charge Accumulation Zone as Photovoltaic Mechanism in Perovskite Solar Cells. *J. Phys. Chem. Lett.* **2016**, *7*, 525−528.
(38) Bergmann, V. W.; Guo, Y.; Tanaka, H.; Hermes, I. M.; Li, D.; Klasen, A.; Bretschneider, S. A.; Nakamura, E.; Berger, R.; Weber, S. A. L. Local Time-Dependent Charging in a Perovskite Solar Cell. *ACS Appl. Mater. Interfaces* **2016**, *8*, 19402−19409.
(39) Chen, Y. F.; Tsai, Y. T.; Bassani, D. M.; Clerc, R.; Forgacs, D.; Bolink, H. J.; Wussler, M.; Jaegermann, W.; Wantz, G.; Hirsch, L. Evidence of Band Bending Induced by Hole Trapping at $MAPbI_3$ Perovskite/Metal Interface. *J. Mater. Chem. A* **2016**, *4*, 17529−17536.

DOI: 10.1021/acsami.7b01306
ACS Appl. Mater. Interfaces 2017, 9, 13181−13187